Materials Physics and Mechanics 42 (2019) 242-255 Received: October 6, 2018

APPLIED THEORY FOR ELECTRO-ELASTIC PLATES WITH NON-HOMOGENEOUS POLARIZATION

A.N. Soloviev[1,2*], V.A. Chebanenko[3], P.A. Oganesyan[2], Shih-Fong Chao[4], Y.-M. Liu[5]

[1]Don State Technical University, Rostov-on-Don, Russia

[2]I.I. Vorovich Mathematics, Mechanics and Computer Science Institute,

Southern Federal University, Rostov-on-Don, Russia

[3]Federal Research Center "Southern Scientific Center of the Russian Academy of Sciences", Rostov-on-Don, Russia

[4]Department of Microelectronics Engineering, National Kaohsiung University of Science and Technology, Kaohsiung, Taiwan

[5]Department of Electric Communication Engineering, National Kaohsiung University of Science and Technology, Kaohsiung, Taiwan

*e-mail: solovievarc@gmail.com

Abstract. Non-uniformly polarized piezoceramic materials can be used in effective energy harvesting devices. Axisymmetric and plane models of electric elastic bodies were studied using applied theory and finite element method (FEM). Applied theory for devices made of parts with longitudinal and transverse polarization was developed. It was based on bending of electric elastic plates models. Numerical experiments for FEM models were performed in ACELAN package. Applied theory of second order vibrations was introduced.
Keywords: functionally graded material (FGM), prescribed temperature, design optimization, residual stresses minimization

1. Introduction

Inhomogenously polarized piezoelectric devices can be designed to outperform homogeneous puzzlements in electro-mechanical properties as electrotechnical coupling coefficient, output voltage and working bandwidth. FEM is one of the most widely used methods in modelling of such devices and solving problems with non-uniformly polarized devices, which requires specific additions. Such analysis can be performed in ACELAN package. In some cases, proper simplifications can be applied to the model, namely some parts with inhomogeneous polarization can be replaced with set of blocks with uniform polarization. Furthermore, applied theory for model is built with uniformly polarized blocks. Such theory was developed for electric elastic plates in plane and axisymmetric problems.

Application of polarization to the device is an important part of manufacturing process. In some cases, parts can be polarized with imperfections as incomplete polarization of deviation of polarization direction. Modeling the polarization process for predefined model geometry and electrode scheme can be performed in ACELAN package. Vector field of the polarization is transferred to finite element meshes and used for solving problems with non-uniform polarization. Difference between simplified block model presented in applied theory and full model solved with FEM is estimated. Some problems can be reduced from full to simplified model without significant accuracy loss. Described programs, models and

http://dx.doi.org/10.18720/MPM.4222019_11

techniques are developed for advanced analysis of non-uniformly polarized energy harvesting devices.

It is known that piezoelectric materials are widely used as actuators, sensors and generators in the engineering and aerospace field for monitoring the state of structures, shape control, active suppression of parasitic vibrations, noise suppression, etc. Such wide application is achieved due to their good electromechanical properties, flexibility in the design process, ease of production, as well as high conversion efficiency, both electrical energy in the mechanical and in the opposite direction. When using piezoelectric materials as actuators, deformations can be controlled by changing the magnitude of the applied electric potential. In the sensors, deformation measurement is also performed by measuring the induced potential. In the field of energy storage by means of piezoelectric materials, the free mechanical energy, that is present in the designs, is converted into electrical energy and then transferred to a suitable low-power device. A detailed survey is given in [1-3].

Typical actuators, sensors and generators, working on bending, are a multi-layered structure consisting of several layers with different mechanical and electrical properties. The conventional design, consisting of two piezoelectric layers, glued to the substrate or to each other, is called a bimorph. More complex multilayered structures are referred already to functional gradient materials.

To model the layered structures, performing as sensors, actuators and generators, various mathematical models were proposed. Thus, in the previous papers [4,5] analytical solutions of the *z*-dimensional equations of the theory of electric elasticity were presented for static cylindrical bending and free vibrations. Nevertheless, the derivation and obtaining of analytic solutions of such equations in the case of arbitrary geometry is a complex problem. Another approach is to use models with induced deformation to simulate the response of the actuator, which were used in [6,7]. However, there the electric potential was not considered as a variable describing the state. This did not allow one to get the related electromechanical responses, but only allowed simulating the response of the actuator. Finite-element models have been proposed in several works, for example, in [8-12]. Some of those models have limitations, the need for large computational resources by using three-dimensional elements in problems, when the thickness of one layer is much less than other design sizes.

In the simulation of piezoelectric designs, the hypothesis of a linear distribution of the electric potential over a thickness is widely used. This means that the induced potential is considered. This is convenient for simulating actuators [13] and piezoelectric generators [14]. Nevertheless, in some materials with a thickness polarization, when an electric field is applied, shear deformations and stresses can arise [12]. In addition, shear stresses and strains arise in multilayer piezoelectric composites [15]. In this connection, accounting for the nonlinear part of the electric potential is of some interest.

In [16], a sandwich model of the third order was considered. The authors have shown that this model gives an additional contribution to rigidity due to the quadratic deformation of the shift and the cubic term of the electric potential. This fact was confirmed by higher natural frequencies. A few papers [17,18] are devoted to the development of a related refined layer-by-layer theory for finite element analysis of multilayer functionally gradient piezoelectric materials. The authors used both the quadratic and cubic electric potential and considered the longitudinal distribution of the potential. This made it possible to consider shear stresses and deformations. We considered forced and free oscillations, which showed good convergence with analytical solutions and commercial FE-software. Nevertheless, the longitudinal distribution of the potential was not presented. In [19] a refined coupled global-local theory was presented for the finite element analysis of thick piezoelectric composites operating on a shear mode. The authors used the quadratic distribution of the thickness potential.

The brief review showed that the use of the nonlinear electric potential distribution, along with considering the longitudinal distribution, is of interest in the problems of calculating multilayer actuators, since it allows more accurate modeling of shear stresses and deformations arising in such structures. Nevertheless, the behavior of the nonlinear electric potential near the resonances has not been sufficiently studied. In connection with this, we developed an applied theory of cylindrical bending of bimorph piezoelectric structures, taking into consideration the quadratic distribution of the thickness potential along with its longitudinal variation.

2. Mathematical model

Both basic coupled electromechanical problem formulation and specific applied theory for second order vibrations are presented in this section.

Let us examine a piezoelectric transducer Ω, presented by a set of areas $\Omega_j = \Omega_{pk}$; $k = 1, 2,..., N_p$; $j = k$ with the properties of piezoelectric materials, and a set of areas $\Omega_j = \Omega_{em}$; $m = 1,2,...,N_e$; $j = N_p + m$ with the properties of elastic materials. It is appropriate to describe the physical-mechanical processes taking place in the media Ω_{pk} and Ω_{em} into framework of piezoelectricity (electric elasticity) and elasticity theory [20,21].

We assume that the following constitutive equations are satisfied (piezoelectric medium is $\Omega_j = \Omega_{pk}$):

$$\rho_{pk}\ddot{\mathbf{u}} + \alpha_{dj}\rho_j\dot{\mathbf{u}} - \nabla\cdot\boldsymbol{\sigma} = \mathbf{f}_j;\ \nabla\cdot\mathbf{D} = 0, \tag{1}$$

$$\boldsymbol{\sigma} = \mathbf{c}_j^E \cdot\cdot(\boldsymbol{\varepsilon} + \beta_{dj}\dot{\boldsymbol{\varepsilon}}) - \mathbf{e}_j^T\cdot\mathbf{E};\ \mathbf{D} + \varsigma_d\dot{\mathbf{D}} = \mathbf{e}_j\cdot\cdot(\boldsymbol{\varepsilon} + \varsigma_d\dot{\boldsymbol{\varepsilon}}) + \mathfrak{э}_j^S\cdot\mathbf{E}, \tag{2}$$

$$\boldsymbol{\varepsilon} = (\nabla\mathbf{u} + \nabla\mathbf{u}^T)/2;\ \mathbf{E} = -\nabla\varphi, \tag{3}$$

where $\rho(\mathbf{x}, t)$ is the continuous function of coordinates (density), $\mathbf{u}(\mathbf{x})$ is the displacement vector-function, $\boldsymbol{\sigma}$ is the stress tensor, $\mathbf{f}$ are the mass forces, $\mathbf{D}$ is the electric induction vector; $\mathbf{c}_j^E$ are the components of the elastic constant tensor; $\mathbf{e}_j^T$ are the piezoelectric stress components, $\boldsymbol{\varepsilon}$ is the strain tensor, $\mathbf{E}$ is the electric field vector; $\varphi(\mathbf{x})$ is the electric potential function; $\mathfrak{э}_j^S$ are the components of the dielectric permittivity tensor; $\alpha_{dj}, \beta_{dj}, \zeta_d$ are non-negative damping coefficients, and the other symbols are the standard designations for theory of electric elasticity with the exception of index j, corresponding to area Ω_j (for elastic media $\Omega_j = \Omega_{ek}$ the piezomoduli $\mathbf{e}_j^T$ are equal to zero).

For the media $\Omega_j = \Omega_{em}$ with pure elastic properties, only stress fields would be considered. Similar Equations (1) – (3) are constitutive relationships, used with neglect electric fields and piezoelectric connectivity effects. Equations (1) – (3) are added to the mechanical and electrical boundary conditions, as well as the initial conditions in the case of non-stationary problem. Numerical modeling of devices that can be described with Equations (1) – (3) is performed by using finite element method.

In addition to previous equations, all material properties are handled as functions of coordinates:

$$\rho_k = \rho_{pk}(\mathbf{x}),\quad \mathbf{c}_j^E = \mathbf{c}_j^E(\mathbf{x}),\quad \boldsymbol{\varepsilon}_{\mathbf{a}j}^S = \boldsymbol{\varepsilon}_{\mathbf{a}j}^S(\mathbf{x}),\quad \mathbf{e}_j^T = \mathbf{e}_j^T(\mathbf{x}); \tag{4}$$

$$g = g^i + |P|(g^a - g^i) \text{ for tensors } \mathbf{c}_j^E \text{ and } \mathfrak{э}_j^S \text{ and } g = |P|g^a \text{ for tensor } \boldsymbol{\varepsilon}_{\mathbf{a}j}^S; \tag{5}$$

here g is corresponding tensor component, i marks isotropic state, a marks anisotropic state. Tensor of piezoelectric constants will be zero for isotropic bodies.

We consider piezoelectric device consisting of two piezoelectric layers and a middle passive layer. The piezoelectric layers are inhomogenously polarized according to the process presented in [22] (Fig. 1).

Fig 1. Inhomogenously polarized ceramic layer

This piezoactive layer has several specific regions with transverse and longitudinal polarization (regions 1, 2 in Fig. 1) and some transition zones from one polarization to another (region 3 in Fig. 1). In [22], an assessment was made of the effect of these transition regions on the characteristics of the piezoelectric device consisting of two piezoactive layers and a comparison was made with the piezoelectric cell shown in Fig. 2a with piecewise inhomogeneous polarization. In the limits of geometrical parameters specified in [22], this simplified model can be used to calculate the output characteristics of a piezoelectric device with non-uniform polarization. In the case of a small thickness in comparison with the characteristic length dimension (which is typical for the full-scale implementation), the static behavior and steady-state oscillations of these piezoelectric devices on the first flexural modes can be described by applied theories. In such theories, a certain distribution of mechanical and electric fields over the thickness of the piezoelectric element is assumed (for example, the invariance of the normal, etc.).

One of the applied theory variants for plane case was described for geometry presented in Fig. 1a. Theory based on studies presented in [3,4] and some implementation details were provided in paper [1]. Model consists from transversally polarized part and longitudinally polarized part with two layers.

Such devices can be made with specific elastic layer to improve mechanical properties. This layer is usually placed between active layers as shown In Fig. 1b. Geometrical parameters of the model are: inner layer thickness h, piezoelectric layers thickness H and lengths L_1 and L_2 for each segment. Median line of the transducer is placed on x-axis for the first segment and on z-axis for the second segment.

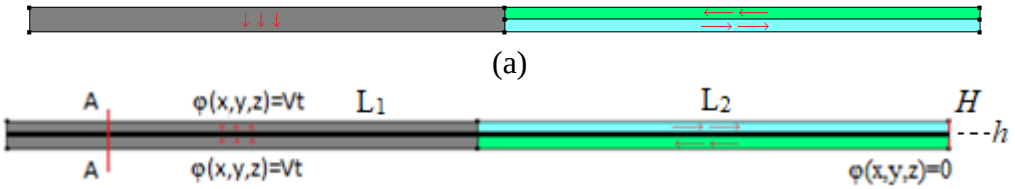

Fig. 2. Device with uniformly polarized parts, initial construction (a) and with medium layer (b)

3. Applied theory

The static deflection was calculated in the finite element package ACELAN for a uniformly distributed normal load and the modal analysis of the piezoelectric element hinged around the edges (determination of frequencies and modes of resonance and antiresonance), presented in Fig. 2b, for h = 1 mm, H = 2 mm $L_1 = L_2$ = 100 mm, piezoelectric PZT-4, steel substrate.

Figure 3 shows the distribution of the transverse displacement under a static load on the deformed state, and Fig. 4 presents distribution of electrical potential.

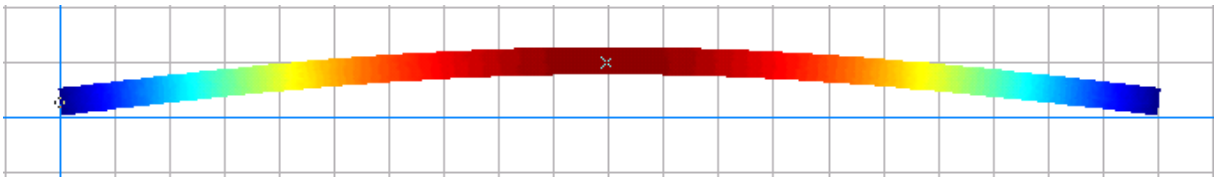

Fig. 3. Vertical component of displacement distribution

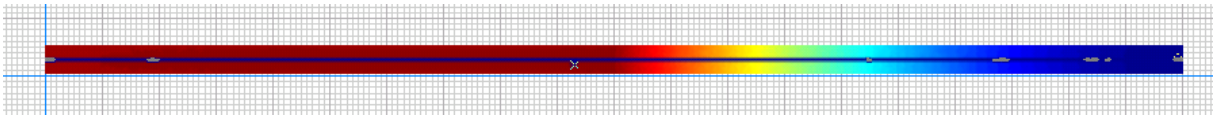

Fig. 4. Electric potential distribution

Figure 5 demonstrates distribution of the electrical potential along the thickness of the upper piezoceramic layer in section A-A (see Fig. 2b).

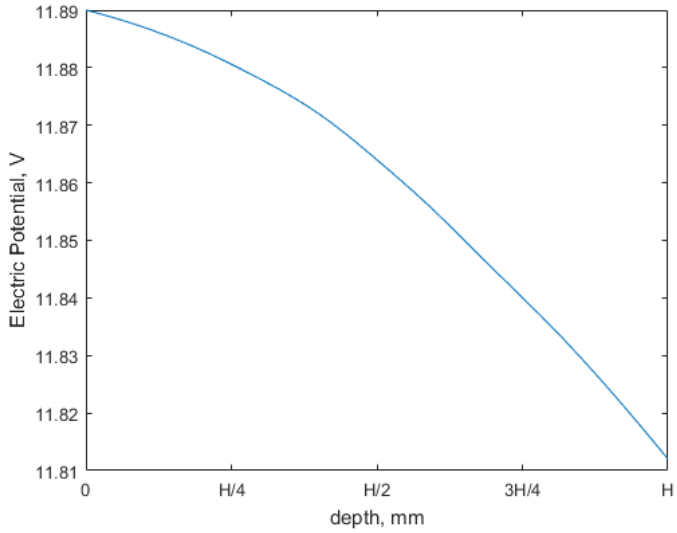

Fig. 5. Distribution of the electrical potential along the thickness of the upper piezoceramic layer in section A-A

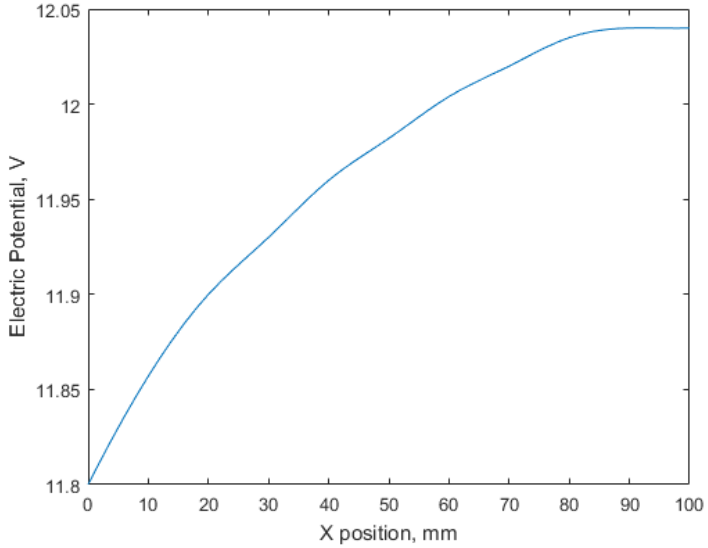

Fig. 6. Distribution along the length of the first section (L_1) of the electric potential at the lower boundary of ceramic layer

Figures 6 and 7 show the distribution along the length of the first section (L_1) of the electric potential at the lower boundary of this layer and in its middle, respectively.

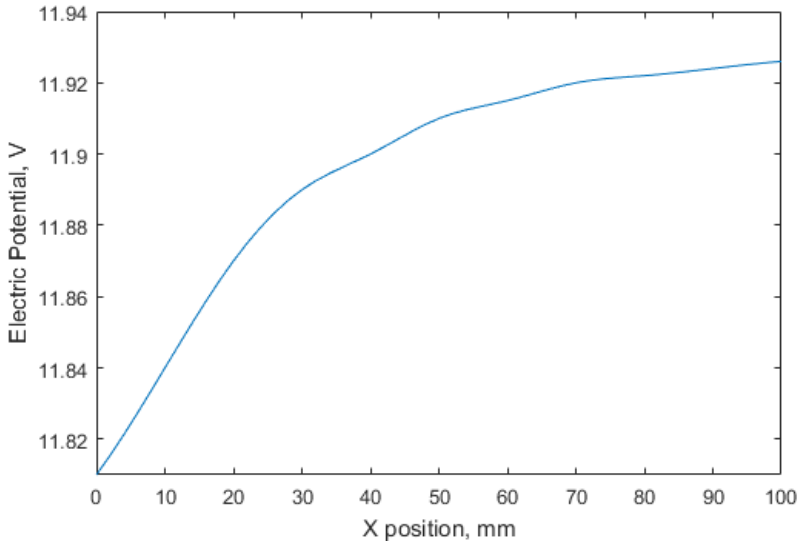

Fig. 7. Distribution along the length of the first section (L_1) of the electric potential at the middle line of ceramic layer

Figures 8 – 11 show results similar to Figs. 4 – 7 for the first resonance $F_r = 0.2049\times10^3$ Hz, and Figs. 12 – 15 for the first antiresonance $F_a = 0.2287\times10^3$ Hz.

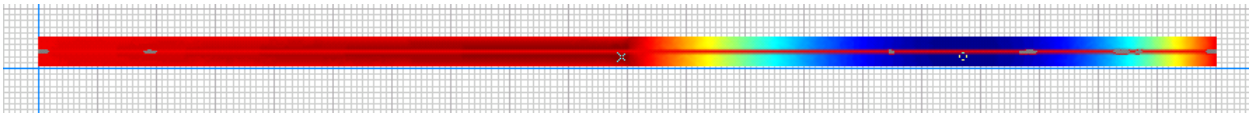

Fig. 8. Potential distribution at resonance frequency

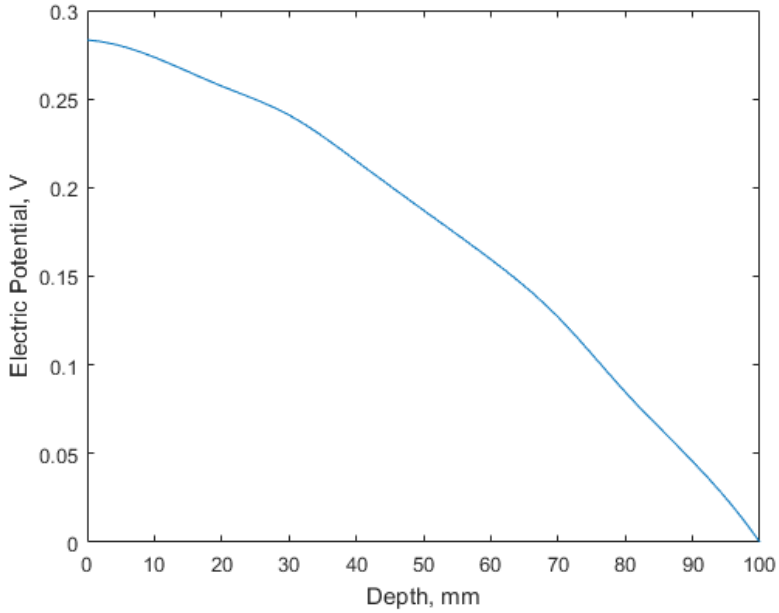

Fig. 9. Distribution of the electrical potential along the thickness of the upper piezoceramic layer in section A-A at resonance frequency

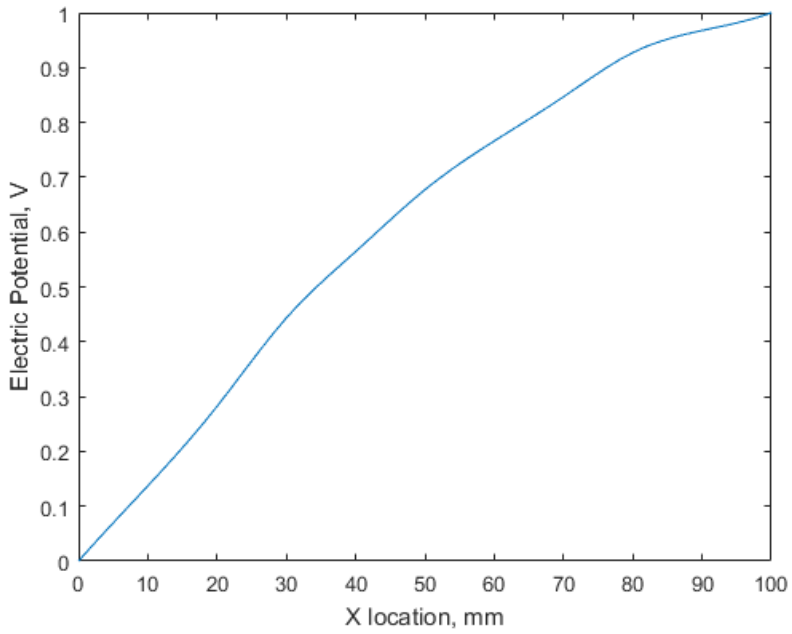

Fig. 10. Distribution along the length of the first section (L_1) of the electric potential at the lower boundary of ceramic layer at resonance

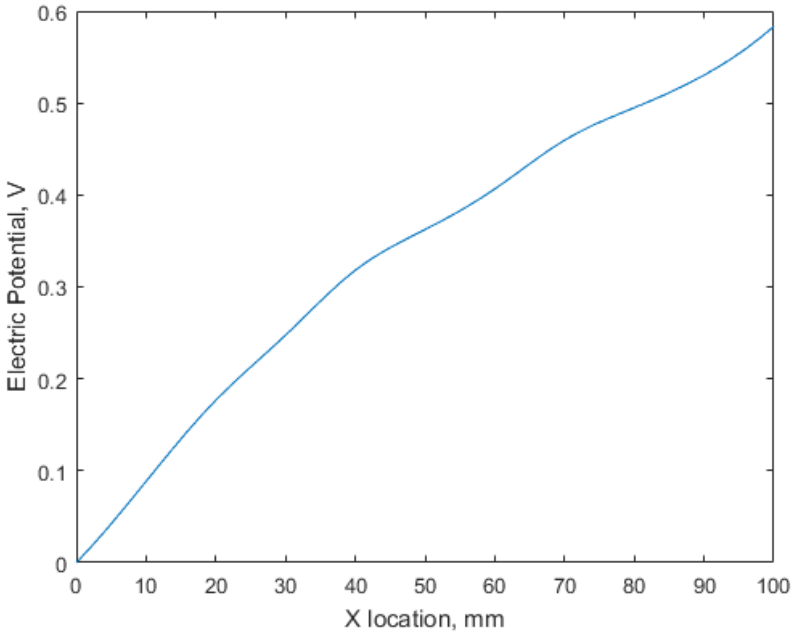

Fig.11. Distribution along the length of the first section (L_1) of the electric potential at the middle line of ceramic layer

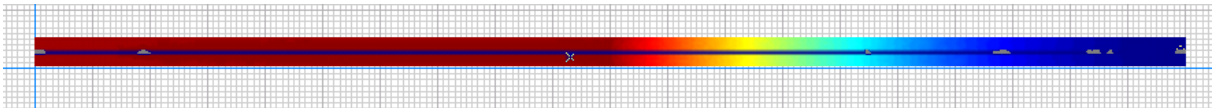

Fig.12. Electric potential distribution at antiresonance frequency

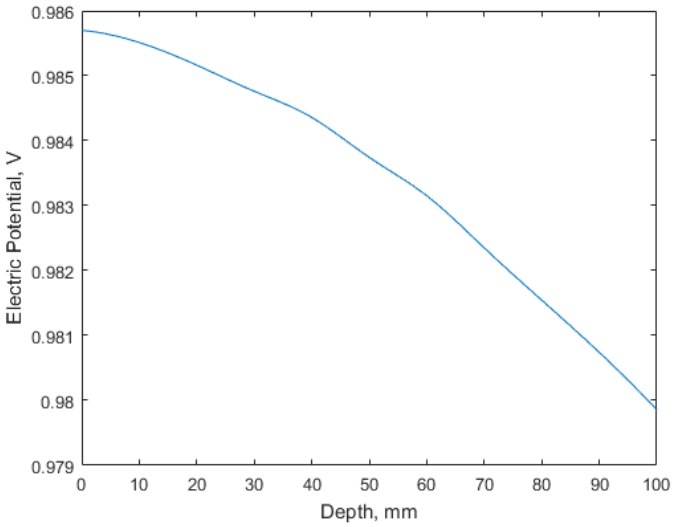

Fig. 13. Distribution of the electrical potential along the thickness of the upper piezoceramic layer in section A-A at antiresonance frequency

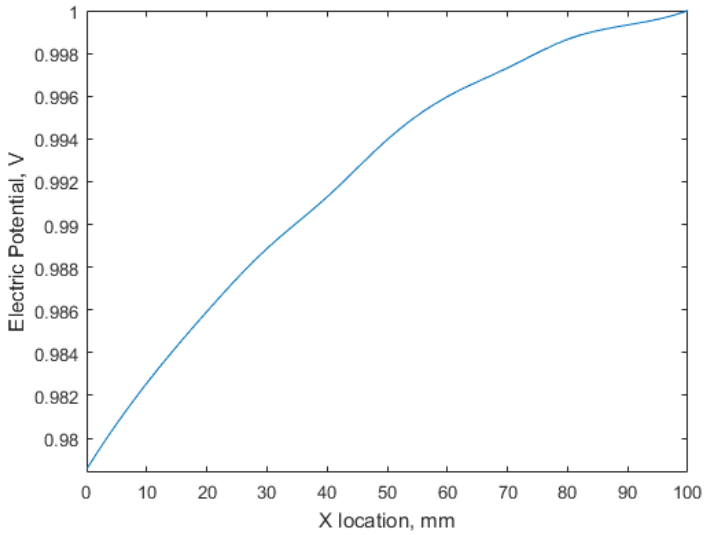

Fig. 14. Distribution along the length of the first section (L_1) of the electric potential at the lower boundary of ceramic layer at antiresonance frequency

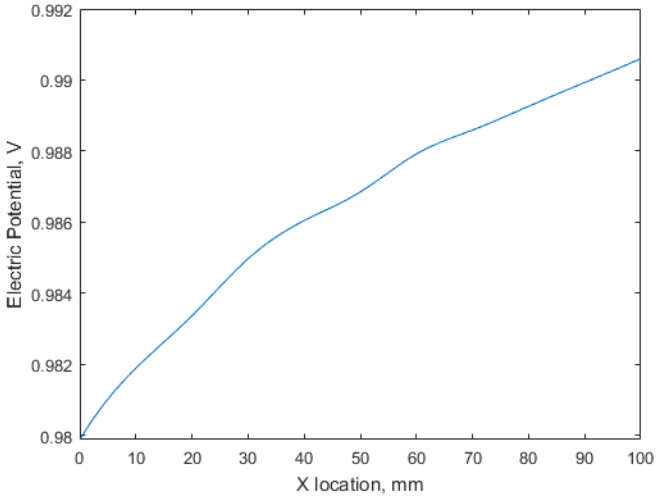

Fig. 15. Distribution along the length of the first section (L_1) of the electric potential at the middle line of ceramic layer at antiresonance frequency

Analysis of numerical results of calculations, including those presented in Figs. 3 – 15 allows us to conclude that the hypothesis of the general normal for the mechanical characteristics of the entire piezoelement is valid. The quadratic law of the electric potential distribution over the thickness in the first fragment of the piezoelement (Fig. 1b) and the constant distribution in the second one is also correct. System of constitutive Equations (2), (3) bending electric elastic plate can be written as follows:

$$\sigma_{11} = c_{11}\varepsilon_{11} + c_{12}\varepsilon_{22} + c_{13}\varepsilon_{33} + e_{31}\frac{\partial\varphi}{\partial z}, \qquad \sigma_{23} = c_{44}(\frac{\partial u_y}{\partial z} + \frac{\partial u_z}{\partial y}) + e_{15}\frac{\partial\varphi}{\partial y},$$

$$\sigma_{22} = c_{12}\varepsilon_{11} + c_{11}\varepsilon_{22} + c_{13}\varepsilon_{33} + e_{31}\frac{\partial\varphi}{\partial z}, \qquad \sigma_{13} = c_{44}(\frac{\partial u_x}{\partial z} + \frac{\partial u_z}{\partial x}) + e_{15}\frac{\partial\varphi}{\partial x},$$

$$\sigma_{33} = c_{13}\varepsilon_{11} + c_{13}\varepsilon_{22} + c_{33}\varepsilon_{33} + e_{33}\frac{\partial\varphi}{\partial z}, \qquad \sigma_{12} = (\frac{c_{11}}{2} - \frac{c_{12}}{2})(\frac{\partial u_x}{\partial y} + \frac{\partial u_y}{\partial z}),$$

$$D_1 = e_{15}(\frac{\partial u_x}{\partial z} + \frac{\partial u_z}{\partial x}) - g_{11}(\frac{\partial\varphi}{\partial x}),$$

$$D_2 = e_{15}(\frac{\partial u_y}{\partial z} + \frac{\partial u_z}{\partial y}) - g_{11}(\frac{\partial\varphi}{\partial y}), \qquad (6)$$

$$D_3 = e_{31}\varepsilon_{11} + e_{31}\varepsilon_{22} + e_{33}\varepsilon_{33} - g_{33}\frac{\partial\varphi}{\partial z},$$

where notations are the same as in (1) – (3).

Elastic layer (black color in Fig. 1b) is an isotropic material with following model, based on model of plates bending [23,24]:

$c_{ii} = \lambda + 2\mu,\ i = 1,2,3;\ c_{ii} = \mu,\ i = 4,5,6;\ c_{ij} = \lambda,\ i \neq j,\ i, j = 1,2,3.$

Assuming $\sigma_{33} = 0$ in a whole volume, ε_{33} can be presented as

$$\varepsilon_{33} = -\frac{c_{13}e_{11} + c_{13}\varepsilon_{22} + e_{33}\frac{\partial\phi}{\partial z}}{c_{33}}. \qquad (7)$$

Assuming a cylindrical bending of the plate and $\varepsilon_{22} = 0$, we have

$$\sigma_{11} = c_{11}\varepsilon_{11} - c_{13}\frac{c_{13}e_{11} + e_{33}\frac{\partial\varphi}{\partial z}}{c_{33}} + e_{31}\frac{\partial\varphi}{\partial z},$$

$$\sigma_{22} = c_{12}\varepsilon_{11} - c_{13}\frac{c_{13}e_{11} + e_{33}\frac{\partial\varphi}{\partial z}}{c_{33}} + e_{31}\frac{\partial\varphi}{\partial z}. \qquad (8)$$

Electric potential distribution for joints on edges of plate is

$$\varphi(x, y, z) = S_1(z)\Phi(x) + S_2(z)\Phi_1(x) + S_3(z)V_t,$$

$$S_1(z) = \frac{1}{4}\frac{(H + h - 2z)(h + 2H - 2z)}{H^2},$$

$$S_2(z) = \frac{(h - 2z)(h + 2H - 2z)}{H^2}, \qquad (9)$$

$$S_3(z) = \frac{1}{4}\frac{(h - 2z)(H + h - 2z)}{H^2},$$

where V_t is constant electric potential value on the electrodes of the plate. $\Phi(x)$ is an electric potential distribution on the bottom surfaces of piezoelectric layers, $\Phi_1(x)$ is an electric potential distribution on the inner middle surfaces of piezoelectric layer.

Displacement distribution variable, in the frame of common normal, can be described as

$$U_x(x,y,z) = -\frac{\partial U_z(x)}{\partial x} \bullet z . \tag{10}$$

Now we can write relations for bending moment M_1 and cutting force Q_1 and D_1:

$$M_1 = \int_{-h/2-H}^{h/2+H} \sigma_{11} z dz = K_1 V_t + K_2 \Phi(x) + K_3 \Phi_1(x) + K_4 \frac{d^2}{dx^2} U_z(x)$$

$$Q_1 = -\frac{\partial M_{11}}{\partial x} = K_5 \frac{\partial}{\partial x}\Phi(x) + K_6 \frac{\partial}{\partial x}\Phi_1(x) + K_4 \frac{d^3}{dx^3} U_z(x)$$

$$C_0 = \frac{c_{13} e_{33}}{c_{33}} - e_{31}$$

$$C_1 = \frac{1}{12}\frac{\mu(\lambda+\mu)h^3}{\lambda+2\mu}$$

$$C_2 = \frac{2H}{3}(c_{11} - \frac{c_{13}^2}{c_{33}})(\frac{3}{4}h^2 + \frac{3}{2}hH + H^2)$$

$$K_1 = -\frac{5}{3}C_0(H + \frac{3}{5}h)$$

$$K_2 = \frac{1}{3}C_0(H + 3h)$$

$$K_3 = \frac{4}{3}C_0 H$$

$$K_4 = C_1 + C_2$$

$$K_5 = -\frac{1}{3}C_0(H + 3h) \tag{11}$$

$$K_6 = -\frac{4}{3}C_0 H$$

$$D_1 = -\frac{1}{3}g_{11}\Phi_1(x) - \frac{4}{3}g_{11}\Phi(x)$$

Equations of oscillations and averaged equation for electric potential:

$$\begin{aligned} &\frac{\partial Q_1}{\partial x} - p(x) - W^2 \rho h U_z(x) = 0, \\ &\int_{-h/2-H}^{h/2+H} (\frac{\partial D_3}{\partial x} + \frac{\partial D_1}{\partial x}) dz = 0, \end{aligned} \tag{12}$$

where ρ is the material density, $p(x)$ is the external force, $W = 2\pi\omega$, ω is the oscillation frequency. After substitution of all known values, (12) becomes:

$$\begin{cases} K_5 \frac{\partial}{\partial x}\Phi(x) + K_6 \frac{\partial}{\partial x}\Phi_1(x) + K_4 \frac{d^4}{dx^4} U_z(x) - W^2 \rho h U_z(x) - p(x) = 0; \\ K_7 V_t + K_7 \Phi(x) - 2K_7 \Phi_1(x) - \frac{1}{3}g_{11}\frac{d^2}{dx^2}\Phi(x) - \frac{4}{3}g_{11}\frac{d^2}{dx^2}\Phi_1(x) + C_0 \frac{d^2}{dx^2} U_z(x) = 0 \end{cases} \tag{13}$$

$$K_7 = -\frac{8}{H^2}(g_{33} + \frac{e_{33}^2}{c_{33}}).$$

From the conditions on the surface of the ceramic layer, we have.

$$V_t = \frac{1}{3L_1}\int_0^{L_1}(4\Phi_1(x)-\Phi(x))dx - \frac{C_0 H(H+2h)}{6L_1(g_{33}+\frac{e_{33}^2}{c_{33}})}\left[\frac{d}{dx}U_z(L_1)-\frac{d}{dx}U_z(0)\right]$$

and

$$K_8 V_t + 3K_8\Phi(x) - 4K_8\Phi_1(x) + \frac{1}{2}hC_0\frac{d^2}{dx^2}U_z(x) = 0\,.$$

For the other part of the transducer, we add local coordinate system with starting point at (L_1, 0). Axes x and z are switched in this local coordinate system. Constitutive equations are the same, at mutually replacing the axes. Potential distribution will be in the next form: $\phi(x,y,z) = \Phi(z)$.

Expressions for D_3, M_3 and Q_3 can be written as follows, using the same technique as in previous part:

$$D_3 = (-\frac{2e_{31}^2}{c_{11}} - 2g_{33})\frac{\partial}{\partial z}\Phi(z) + (-\frac{2e_{31}^2 x}{c_{11}} - 2g_{33}x)\frac{\partial^2}{\partial z^2}U_x(z)$$

$$M_3 = \frac{1}{2}(-\frac{2c_{13}e_{31}}{c_{11}} + 2e_{33})((\frac{1}{2}h+H)^2 - \frac{1}{4}h^2)\frac{\partial}{\partial z}\Phi(z) +$$

$$+\frac{1}{3}(\frac{2c_{13}^2}{c_{11}} - 2c_{33})((\frac{1}{2}h+H)^3 - \frac{1}{8}h^3)\frac{\partial^2}{\partial z^2}\Phi(z) \qquad (14)$$

$$Q_3 = -\frac{1}{2}(-\frac{2c_{13}e_{31}}{c_{11}} + 2e_{33})((\frac{1}{2}h+H)^2 - \frac{1}{4}h^2)\frac{\partial^2}{\partial z^2}\Phi(z) +$$

$$+(-\frac{1}{3}(\frac{2c_{13}^2}{c_{11}} - 2c_{33})((\frac{1}{2}h+H)^3 - \frac{1}{8}h^3) - \frac{1}{24}(-2\lambda - 4\mu + \frac{2\lambda^2}{\lambda+2\mu})h^3)\frac{\partial^3}{\partial z^3}U_x(z).$$

By using (14) Equations (12) reduce to the following form:

$$\begin{cases} -\frac{1}{2}(-\frac{2c_{13}e_{31}}{c_{11}} + 2e_{33})((\frac{1}{2}h+H)^2 - \frac{1}{4}h^2)(\frac{\partial^3}{\partial z^3}\Phi(z)) + (-\frac{1}{3}(\frac{2c_{13}^2}{c_{11}} - 2c_{33})((\frac{1}{2}h+H)^3 - \frac{1}{8}h^3) - \\ -\frac{1}{24}(-2\lambda - 4\mu + \frac{2\lambda^2}{\lambda+2\mu})h^3)(\frac{\partial^4}{\partial z^4}U_x(z)) - W^2\rho h U_x(z) - p(y,z) = 0; \qquad (15) \\ (-\frac{2e_{31}^2}{c_{11}} - 2g_{33})\frac{\partial^2}{\partial z^2}\Phi(z) + \frac{(\frac{c_{13}e_{31}}{c_{11}} - e_{33})((\frac{1}{2}h+H)^2 - \frac{1}{4}h^2)\frac{\partial^3}{\partial z^3}U_x(z)}{H} = 0. \end{cases}$$

General solutions of these linear differential equations can be found with common methods. Upper indices 1 and 2 will be used to mark the first and the second parts of the transducer. So, $U^1(x)$ and $\Phi^1(x)$ will be solutions for (13); U^2(x) and $\Phi^2(x)$ will be solutions for (15).

Let us consider the conditions under which hard fixation and zero potential are given at the left and right ends of the transducer, and the equality of the fields is established at the junction of the ceramics with different polarization. Writing the boundary conditions in local coordinates for joints on edges of plate, we obtain the following set of twelve equations:

$$
\begin{aligned}
&U^1(0)=0 && U^1(L_1)=U^2(0)\\
&M^1(0)=0 && M^1(L_1)=M^2(0)\\
&\frac{1}{3}g_{11}\Phi_1(0)-\frac{4}{3}g_{11}\Phi(0)=0 && \Theta^1(L_1)=\Theta^2(0)\\
& && Q^1(L_1)=Q^2(0)\\
&U^2(L_2)=0 && \frac{1}{3}V_t+\frac{1}{3}\Phi(L_1)+\frac{4}{3}\Phi_1(L_1)=\Phi^2(0)\\
&M^2(L_2)=0 && \frac{1}{H}(\frac{1}{3}g_{11}\Phi_1(L_1)-\frac{4}{3}g_{11}\Phi(L_1))=D_3(0)\\
&\Phi^2(L_2)=0 &&
\end{aligned}
\qquad (16)
$$

The boundary conditions (16) allow us, using solution of equations (13), (15), to write down a system of linear algebraic equations and calculate the integration constant. Applied theory for the asymmetrical part (Fig. 3) can be obtained in same manner. Geometry and material properties were parametrized in Maple software to enable automation of numerical experiments.

4. Numerical experiments

Numerical experiments were carried out with the help of the developed model of cylindrical bending of a three-layer piezoelement (Fig. 1b) with piecewise homogeneous piezoceramic layers. We estimated the influence of the ratio of the sizes of the first and second fragments and methods of fixing them at the ends on resonance frequencies, antiresonance, electromechanical coupling coefficient (EMCC) and output potential V_t at static load. So, these results are presented in Table 1 for a pinned piezoelement.

Table 1. Results for joint connection

L_1, mm	F_r, kHz	F_a, kHz	EMCC	Electric potential, V
180	0.2274	0.2276	0.042	0.08334
160	0.2253	0.2277	0.145	0.6331
140	0.2206	0.2279	0.251	1.966
120	0.2133	0.2282	0.355	8.291
100	0.2049	0.2287	0.444	11.81
80	0.1971	0.2292	0.510	15.34
60	0.1910	0.2297	0.555	18.59
40	0.1873	0.2300	0.580	21.27
20	0.1862	0.2302	0.588	23.10

Tables 2 and 3 present results for a piezoelectric element rigidly fixed at the right and left ends, respectively, with the second line corresponding to the hinge fixation, the third fixing of the substrate only, and last fixing both the substrate and the piezoceramic layers.

Table 2. Right fixation

L_1 = 100 mm	F_r, kHz	F_a, kHz	EMCC	Electric potential, V
Joint	0.2049	0.2287	0.444	11.81
Substrate only	0.2961	0.2980	0.113	2.591
Ceramics and substrate	0.3554	0.3571	0.097	1.588

Table 3. Left fixation

L_1 = 100 mm	F_r, kHz	F_a, kHz	EMCC	Electric potential, V
Joint	0.2049	0.2287	0.444	0.2287
Substrate only	0.2736	0.3045	0.439	0.3045
Ceramics and substrate	0.3185	0.3571	0.452	0.3571

5. Conclusions

Presented tools and models can be used for analysis of electric elastic materials in different types of transducers, including energy harvesting devices. Due to greater output voltage and wider bandwidth such devices are more effective then uniformly polarized transducers. In some cases, models can be reduced to simplified uniformly polarized blocks and further to theoretical solutions.

Numerical experiments have shown that pivoting of the piezoelectric element is most preferable. The output potential and EMCC increases with the decrease in the relative size of the first fragment, but it is obvious that the capacity decreases.

Acknowledgements. *This research was supported by grant RFBR number 16-01-00354 A.*

References

[1] Gaudenzi P. *Smart Structures: Physical Behavior, Mathematical Modeling and Applications*. New York: John Wiley & Sons; 2009.

[2] Chopra I. Review of state of art of smart structures and integrated systems. *AIAA J.* 2002;40(11): 2145-2187.

[3] Chebanenko VA, Akopyan VA, Parinov IA. Piezoelectric Generators and Energy Harvesters: Modern State of the Art. In: Parinov IA. (ed.) *Piezoelectrics and Nanomaterials: Fundamentals, Developments and Applications.* New York: Nova Science Publishers; 2015. p.243-277.

[4] Ray MCH, Rao KM, Samanta B. Exact solution for static analysis of an intelligent structure under cylindrical bending. *Comput. Struct.* 1993;47(6): 1031-1042.

[5] Heyliger PR, Brooks SB. Free vibration of piezoelectric laminates in cylindrical bending. *Int J Solids Struct*. 1995;32(20): 2945-2960.

[6] Sung CK, Chen TF, Chen SG. Piezoelectric modal sensor/actuator design for monitoring/generating flexural and torsional vibrations of cylindrical shells. *J Sound Vib.* 1996;118(1): 48-55.

[7] Saravanos DA, Heyliger PR. Mechanics and computational models for laminated piezoelectric beams, plates, and shells. *Appl Mech Rev*. 1999;52(10): 305-320.

[8] Allik H, Hughes TJR. Finite element method for piezoelectric vibration. *Int J Numer Methods Eng.* 1970;2(2): 151-157.

[9] Benjeddou A. Advances in piezoelectric finite element modeling of adaptive structural elements: a survey. *Computers & Structures.* 2000;76(1-3): 347-363.

[10] Sheikh AH, Topdar P, Halder S. An appropriate FE model for through thickness variation of displacement and potential in thin/moderately thick smart laminates. *Compos Struct.* 2001;51(4):401-409.

[11] Kogl M, Bucalem ML. Analysis of smart laminates using piezoelectric MITC plate and shell elements. *Comput Struct*. 2005;83(15-16): 1153-1163.

[12] Benjeddou A, Trindade MA, Ohayon RA. A unified beam finite element model for extension and shear piezoelectric actuation mechanisms. *J Intell Mater Syst Struct.* 1997;8(12): 1012-1025.

[13] Maurini C, Pouget J, Dell'Isola F. Extension of the Euler–Bernoulli model of piezoelectric laminates to include 3D effects via a mixed approach. *Computers & structures.* 2006;84(22-23): 1438-1458.
[14] Soloviev AN, Chebanenko VA, Parinov IA. Mathematical Modelling of Piezoelectric Generators on the Base of the Kantorovich Method. In: Altenbach H, Carrera E, Kulikov G. (eds.) *Analysis and Modelling of Advanced Structures and Smart Systems.* Singapore: Springer; 2018. p.227-258.
[15] Kapuria S, Kumari P, Nath JK. Efficient modeling of smart piezoelectric composite laminates: a review. *Acta Mechanica*. 2010;214(1-2): 31-48.
[16] Trindade MA, Benjeddou A. Refined sandwich model for the vibration of beams with embedded shear piezoelectric actuators and sensors. *Computers & Structures.* 2008;86(9): 859-869.
[17] Beheshti-Aval SB, Lezgy-Nazargah M. Coupled refined layerwise theory for dynamic free and forced response of piezoelectric laminated composite and sandwich beams. *Meccanica*. 2013;48(6): 1479-1500.
[18] Lezgy-Nazargah M, Vidal P, Polit O. An efficient finite element model for static and dynamic analyses of functionally graded piezoelectric beams. *Composite Structures*. 2013;104: 71-84.
[19] Beheshti-Aval SB, Shahvaghar-Asl S, Lezgy-Nazargah M, Noori M. A finite element model based on coupled refined high-order global-local theory for static analysis of electromechanical embedded shear-mode piezoelectric sandwich composite beams with various widths. *Thin-Walled Structures*. 2013;72: 139-163.
[20] Soloviev AN, Oganesyan PA, Skaliukh AS, Duong LV, Gupta VK, Panfilov IA. Comparison Between Applied Theory and Finite Element Method for Energy Harvesting Non-homogeneous Piezoelements Modeling. In: Parinov IA, Chang SH, Jani MA. (eds.) *Advanced Materials Techniques, Physics, Mechanics and Applications.* Springer Proceedings in Physics book series (SPPHY, volume 173). Cham: Springer; 2017. p.473-484.
[21] Belokon AV, Eremeyev VA, Nasedkin AV, Solov'yev AN. Partitioned schemes of the finite element method for dynamic problems of acoustoelectroelasticity. *Journal of Applied Mathematics and Mechanics*. 2000;64(3): 367-377.
[22] Soloviev AN, Oganesyan PA, Lupeiko TG, Kirillova EV, Chang S-H, Yang C-D. Modeling of Non-uniform Polarization for Multi-layered Piezoelectric Transducer for Energy Harvesting Devices. *Advanced Materials: Manufacturing, Physics, Mechanics and Applications.* Springer Proceedings in Physics book series (SPPHY, volume 175). Cham: Springer; 2016. p.651-659.
[23] Vatulian AO, Getman IP, Lapnitskaya NB. About the bending of piezoelectric bimorph plate. *Applied Mechanics*. 1991;27(10): 101-105.
[24] Vatul'yan AO, Rynkova AA. Flexural Vibrations of a piezoelectric bimorth with a Cut Internal Electrode. *Journal of Applied Mechanics and Technical Physics*. 2001;42(1): 164-168.